

Emergence of Exotic Spin Texture in Supramolecular Metal Complexes on a 2D Superconductor

Viljam Vaño,¹ Stefano Reale,^{2,3,4} Orlando J. Silveira,¹ Danilo Longo,⁵ Mohammad Amini,¹ Massine Kelai,^{2,3} Jaehyun Lee,^{2,6} Atte Martikainen,⁷ Shawulienu Kezilebieke,⁸ Adam S. Foster,^{1,9} Jose L. Lado,¹ Fabio Donati,^{2,6,*} Peter Liljeroth,^{1,*} and Linghao Yan^{10,11,1,*}

¹*Department of Applied Physics, Aalto University, FI-00076 Aalto, Finland*

²*Center for Quantum Nanoscience (QNS),*

Institute for Basic Science (IBS), Seoul 03760, Republic of Korea

³*Ewha Womans University, Seoul 03760, Republic of Korea*

⁴*Department of Energy, Politecnico di Milano, Milano 20133, Italy*

⁵*CIC nanoGUNE-BRTA, 20018 Donostia-San Sebastián, Spain*

⁶*Department of Physics, Ewha Womans University, Seoul 03760, Republic of Korea*

⁷*Department of Physics, P.O. Box 4, FI-00014 University of Helsinki, Finland*

⁸*Department of Physics, Department of Chemistry and Nanoscience Center, University of Jyväskylä, FI-40014 University of Jyväskylä, Finland*

⁹*WPI Nano Life Science Institute (WPI-NanoLSI),*

Kanazawa University, Kakuma-machi, Kanazawa 920-1192, Japan

¹⁰*Institute of Functional Nano & Soft Materials (FUNSOM), Soochow University, Suzhou, 215123, Jiangsu, PR China*

¹¹*Jiangsu Key Laboratory for Carbon-Based Functional Materials & Devices, Soochow University, Suzhou, 215123, Jiangsu, PR China*

(Dated: September 7, 2023)

Designer heterostructures, where the desired physics emerges from the controlled interactions between different components, represent one of the most powerful strategies to realize unconventional electronic states [1, 2]. This approach has been particularly fruitful in combining magnetism and superconductivity to create exotic superconducting states [3–6]. In this work, we use a heterostructure platform combining supramolecular metal complexes (SMCs) with a quasi-2D van der Waals (vdW) superconductor NbSe₂. Our scanning tunneling microscopy (STM) measurements demonstrate the emergence of Yu-Shiba-Rusinov (YSR) bands arising from the interaction between the SMC magnetism and the NbSe₂ superconductivity. Using X-ray absorption spectroscopy (XAS) and X-ray magnetic circular dichroism (XMCD) measurements, we show the presence of antiferromagnetic coupling between the SMC units. These result in the emergence of an unconventional 3×3 reconstruction in the magnetic ground

state that is directly reflected in real space modulation of the YSR bands. The combination of flexible molecular building blocks, frustrated magnetic textures, and superconductivity in heterostructures establishes a fertile starting point to fabricating tunable quantum materials, including unconventional superconductors and quantum spin liquids.

Supramolecular metal complexes (SMCs) are a highly versatile class of metal-organic materials that combine flexible design, widely tuneable properties and facile access to large scale structures via molecular self-assembly [7]. The ability to tune the lattice geometry, the magnetism and spin-orbit coupling arising from the metal atoms within these complexes, along with the diverse interactions with the substrate, has led to the prediction of a multitude of extraordinary electronic properties exhibited by SMCs [8, 9]. Only a handful of these effects has been realized in practice, including the manifestation of magnetic properties [10, 11], surface-state engineering [12], and realizing structures potentially hosting topologically non-trivial band structures [13].

While SMCs can host intrinsic exotic states, creating heterostructures with proximity effects offers even more possibilities. For example, combining magnetic impurities with superconductivity can give rise to Yu-Shiba-Rusinov (YSR) states [14–16]. Arranging such impurities in 1D and 2D lattices together with a suitable magnetic texture and spin-orbit interactions provides a route to various artificial topological superconducting states [3, 4, 17–21]. Even though YSR bands have been successfully achieved in assemblies of individual magnetic atoms, and with inorganic chains and layers [6, 22–25], the emergence of YSR bands in molecular systems still remains elusive [26–29]. The downside of this approach is that molecular systems on typical bulk superconducting substrates combine the large lattice constants of SMCs with small YSR orbitals. This leads to very limited overlap between the YSR states, hindering the potential creation of YSR bands. In addition, magnetic coupling between the SMC building blocks is typically small.

NbSe₂ has been shown to host YSR states with spatially extended orbitals due to its quasi-2D character [30–32]. We demonstrate that this allows for a significant overlap of the YSR states in SMC/NbSe₂ heterostructures resulting in the formation of robust YSR bands. Furthermore, we show the presence of antiferromagnetic coupling within the SMC layer by synchrotron-based X-ray absorption spectroscopy (XAS) and magnetic circular dichroism (XMCD). Together with the triangular SMC lattice, this results in magnetic frustration giving rise to an unconventional 3×3 reconstruction in the magnetic ground state. This modulation is directly reflected in the local-density of states (LDOS) of the YSR bands that we probe via scanning tunneling microscopy (STM)

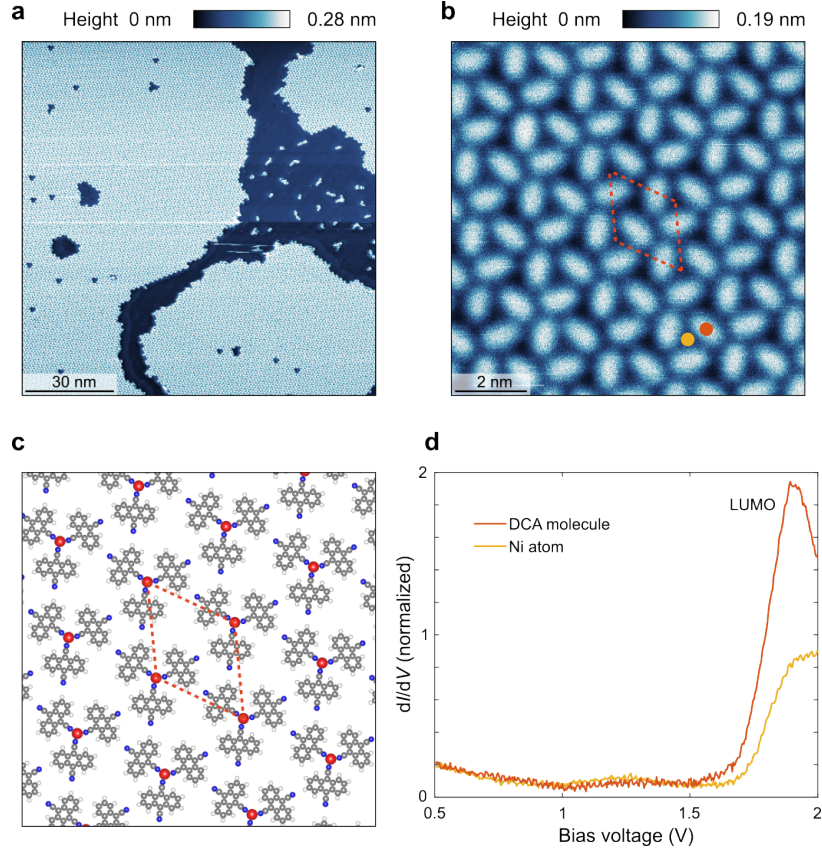


FIG. 1. **Magnetic NiDCA₃ SMC on superconducting NbSe₂.** **a,b**, Large area STM image (**a**, $V = 1.73$ V and $I = 10$ pA) and small area STM image (**b**, $V = 1$ V and $I = 5$ pA) of NiDCA₃ SMC on NbSe₂. **c**, DFT calculated structure of the NiDCA₃ SMC on the NbSe₂ substrate (substrate atoms not shown). **d**, dI/dV spectra measured on top of the DCA molecule (orange) and Ni atom (yellow) within the NiDCA₃ SMC.

and spectroscopy (STS). The successful synthesis of magnetically coupled SMC on NbSe₂ and the formation of YSR bands thus provides an archetypal platform for engineering unconventional quantum phases in SMC/superconductor hybrid systems.

Heterostructure of NiDCA₃ on NbSe₂

The STM image in Fig. 1a shows the results of the growth of a single-layer NiDCA₃ (DCA = dicyanoanthracene) SMC on NbSe₂ (details of the sample preparation are given in the Methods Section). The bright areas are self-assembled SMC islands extending over tens of nanometers, with smaller size SMC clusters randomly distributed between them. A smaller area STM image (Fig. 1b) reveals the triangular lattice of the SMC, which has the structure matching the density

functional theory (DFT) calculations shown in Fig. 1c. The building unit of the SMC consists of three DCA molecules surrounding a Ni atom, forming a NiDCA₃ single complex arranged in a triangular lattice. This metal coordination is similar to the earlier results on Co-DCA and Cu-DCA networks on graphene and NbSe₂ and in a stark contrast with the close-packed assembly of pure DCA molecules on NbSe₂ [33–35]. The magnetic Ni atoms create a triangular lattice of magnetic impurities on the superconducting NbSe₂ substrate (Fig. 1c), with an experimentally determined lattice constant of 2.03 nm that matches the value of 2.07 nm calculated by DFT (see Supplementary Information (SI) for details). The dI/dV spectra taken on top of Ni atom and DCA molecules show a broad peak between 1.5 V and 2 V (Fig. 1d), representing the typical metal-ligand bonding orbital features formed in the single complex (see Fig. S1 in the SI) [33, 36].

Emergence of Yu-Shiba-Rusinov bands

A single magnetic impurity on top of a superconductor induces a pair of YSR states inside the superconducting gap (Fig. 2a) [14–16, 22]. Analogous to the electronic lattice, the overlap of YSR states leads to their hybridization and thus to the formation of YSR bands. These appear as broad features in the spectral function rather than the sharp peaks stemming from single states, as illustrated in Fig. 2d. We investigated this using STM with a superconducting NbSe₂ tip that improves the energy resolution of the experiment and more importantly, the stability of the measurements on the molecular assemblies (see Methods and SI for details). Our experimental observations on SMCs on NbSe₂ confirm the expected transition from single YSR states to YSR bands: when an isolated single complex is positioned on NbSe₂ (Fig. 2b), two sharp peaks appear in the tunneling spectroscopy symmetrically around the Fermi level, as shown in Fig. 2c. As these single complexes form a SMC lattice (Fig. 2e), the sharp peaks in the tunneling spectrum become broader and weaker in intensity (Fig. 2f). This is a sign of strong hybridization and a band formation, which is enabled by the large spatial extent of YSR states of NbSe₂ [30–32] and leads to a significant overlap of these states between neighbouring single complexes. Another sign of YSR band formation, as we will show in the following, is that there is a strong YSR LDOS across the whole unit cell of the SMC.

One of the advantages of our work, stemming from the large unit cell and extended YSR orbitals, is the further insight into spatial behavior of the YSR bands when probed by STM. This can reveal information about the orbital nature of the electronic state that induces the YSR state. While numerous studies have reported this for coupled YSR dimers and chains, research efforts

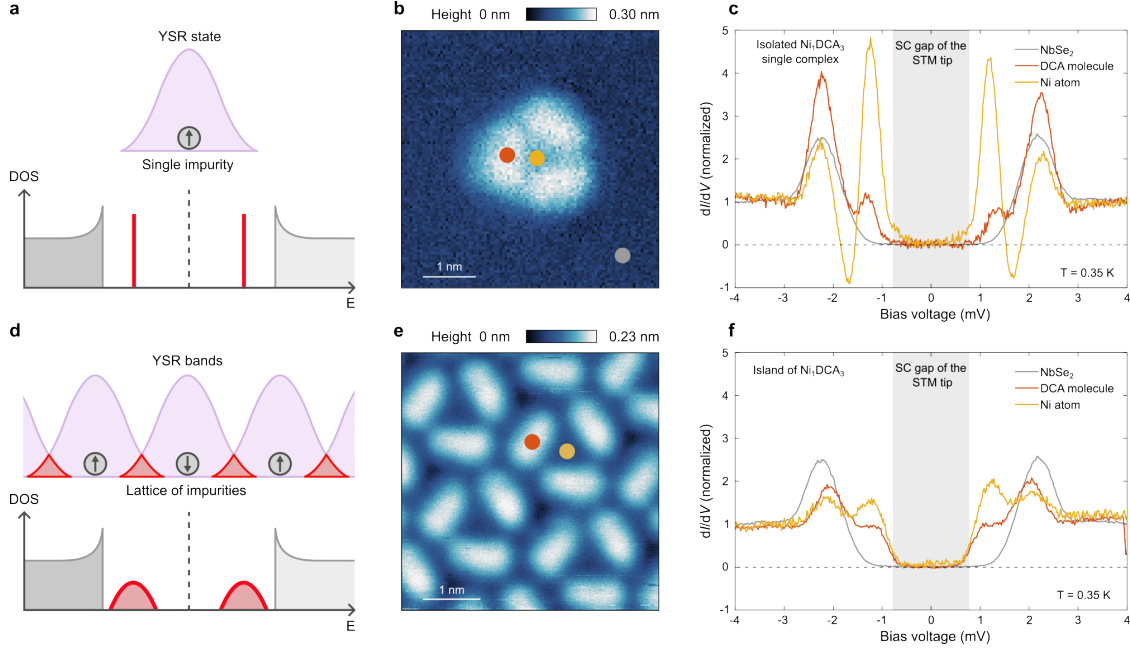


FIG. 2. Evolution from a single magnetic impurity to a lattice of magnetic impurities. **a**, Schematics of a single magnetic impurity interacting with a superconductor, which leads to YSR states represented by two sharp peaks in the DOS. **b**, STM image of isolated NiDCA₃ single complex ($V = 1$ V and $I = 5$ pA). **c**, dI/dV spectra measured with a superconducting tip on NbSe₂ (gray) and on Ni atom (yellow) and DCA molecule (orange) of the isolated NiDCA₃ single complex. **d**, Schematics of lattice of magnetic impurities interacting with a superconductor, which leads to YSR bands and broad in-gap features in the DOS. **e**, STM image of NiDCA₃ SMC on NbSe₂ ($V = 1$ V and $I = 10$ pA). **f**, dI/dV spectra measured with superconducting NbSe₂ tip on NbSe₂ (gray) and on the Ni (yellow) and DCA (orange) within the NiDCA₃ SMC.

focused on 2D YSR lattices remain notably limited [24, 25]. The LDOS map in Fig. 3b visualizes the YSR band, which was measured on the area shown in Fig. 3a. The intensity of the YSR bands is particularly concentrated around the central Ni atom of each single complex, where DFT finds maximal spin density. However, due to the remarkable spatial extent of the YSR states, a pronounced intensity pattern is visible across the whole unit cell even where the spin density vanishes (Figs. 3c,e). The additional long-range modulation of the YSR band occurring over several unit cells shown in Fig. 3a is due to a magnetic ground state, as we show later in the text.

Magnetism of Ni atoms from XAS and XMCD

To gain insight into the electronic configuration of the Ni atoms in the SMC, XAS and XMCD measurements were conducted at the DEIMOS beamline of the SOLEIL synchrotron (details in

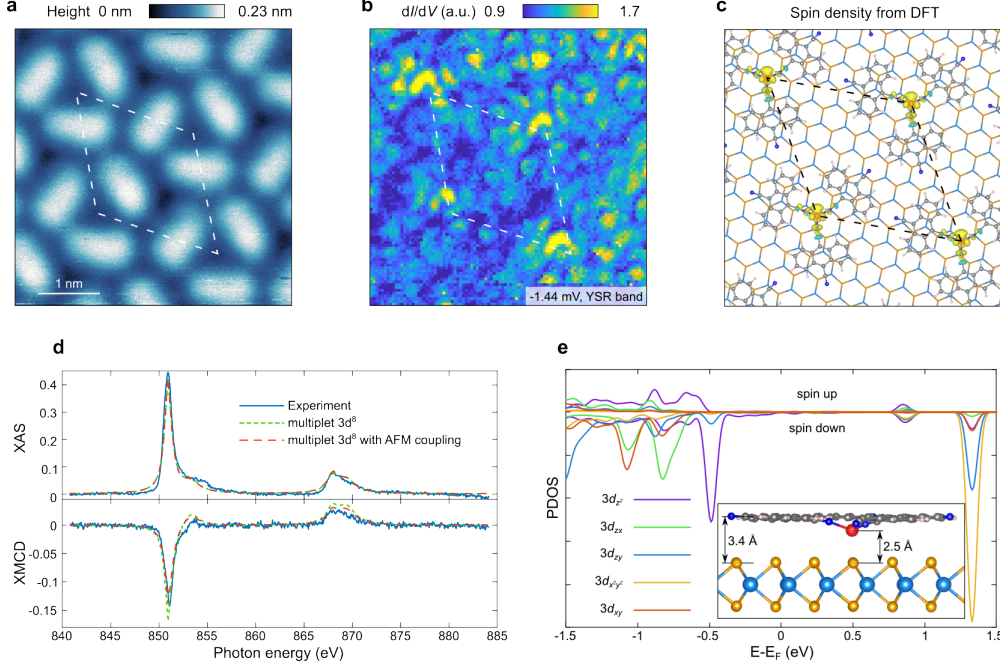


FIG. 3. **Spatial distribution of the YSR bands and electronic configuration of the Ni.** **a**, STM image of NiDCA₃ SMC on NbSe₂ ($V = 1$ V and $I = 10$ pA). **b**, dI/dV map of the area shown in (a) at $V = -1.44$ mV, corresponding to the energy of the YSR band ($V_{\text{mod}} = 100$ μ V). **c**, Spatial distribution of the spin density of NiDCA₃/NbSe₂, calculated by DFT. **d**, XAS and corresponding XMCD of the NiDCA₃/NbSe₂ at the Ni $L_{2,3}$ edges. Experiments (blue lines) are compared with multiplet calculations performed for a $3d^8$ configuration neglecting (green dashed lines) or including (red dashed lines) a magnetic coupling among the Ni centers, see text for more details ($T_{\text{sample}} = 1.9$ K, magnetic field $B = 6.0$ T). **e**, PDOS of Ni 3d orbitals within the NiDCA₃ SMC, calculated by DFT.

the Methods section). Figure 3d shows the spectra collected at the $L_{2,3}$ edges of Ni exhibiting a characteristic $3d^8$ lineshape [37]. The large XMCD signal indicates a high spin configuration with a triplet $S = 1$ ground state. Angular-dependent XAS and XMCD measurements reveal a weak magnetic anisotropy, with a greater magnetization along the out-of-plane direction (see SI). To quantitatively analyze the magnetic state of the Ni atoms, we performed a fitting procedure using simulated spectra based on atomic multiplet calculations. The calculations considered a Ni $3d^8$ configuration, accounting for intra-atomic electron-electron interactions, spin-orbit coupling, crystal field effects within the C_{3v} symmetry, and an external magnetic field (see Methods). The result of the fit, overlaid to the experiment in Fig. 3d, supports the inferred $3d^8$ configuration with a $S = 1$ triplet ground state and allows quantifying a value for the magnetic anisotropy of about 0.1 meV. While the multiplet model nicely reproduces the shape of both XAS and XMCD spectra, the amplitude of the XMCD signal appears to be slightly overestimated. As discussed in

the following section, the inclusion of antiferromagnetic interactions between the Ni atoms enables a comprehensive reproduction of the XMCD amplitude at all magnetic fields and temperatures. Additionally, we computed the projected density of states (PDOS) for the Ni d-orbitals (Fig. 3e) by DFT and determined the orbital occupation of $3d^8$ magnetic state for the Ni atoms based on inputs from X-ray absorption spectroscopy (Fig. 3d). These results demonstrate that the studied SMC realizes a $S = 1$ lattice.

To unravel the nature and strength of the magnetic interactions in the SMC, we acquired magnetization loops by measuring the XMCD signal (Fig. 3d, down) while sweeping the applied magnetic field over a range between -6 and +6 T, and at temperatures from 2 to 50 K. The curve acquired at 2 K shown in Fig. 4a shows a smooth reversible loop, with no hysteresis or magnetization jumps between the backward and forward branch indicating the absence of stable magnetic structures at that temperature. However, the amplitude and slope of the curve are lower than the expected values of a $S = 1$ Brillouin function at $T = 2.0$ K (black solid line). Including the full multiplet structure (red solid line) only marginally improves the discrepancy between experiment and theory. The same type of discrepancy appears in the magnetic susceptibility extracted from the magnetization loops as a function of temperature (see Fig. 4b), with both $S = 1$ Brillouin and full multiplet model not capturing the experimental trend. The model improves remarkably by assuming the presence of antiferromagnetic interactions through n nearest-neighbor pairwise exchange J^{ex} resulting in a Curie-Weiss temperature $T_{CW} = -\frac{S(S+1)}{3k_B}nJ^{ex}$ [38], which we take as a free parameter of the fit (green solid line). The combination of multiplet calculations and the just mentioned antiferromagnetic interaction provides an excellent agreement with the experiment for a $T_{CW} = -2.5$ K, which corresponds to an exchange energy of about 0.2 meV. This indicates that the exchange interaction between the Ni atoms dominates over the magnetic anisotropy. The relation between T_{CW} and the ordering Néel temperature T_N depends on the geometry of the spin lattice and on the neighbor order contributing to the magnetic coupling. For the case of a frustrated triangular-type lattice where only the first nearest neighbors are considered [38], $T_N = -T_{CW}/2 = 1.25$ K, i.e., lower than the base temperature for XMCD measurements, in line with what was observed above. The low Curie-Weiss and Néel temperatures are consistent with the relatively large distances and absence of chemical bonds between the single complexes.

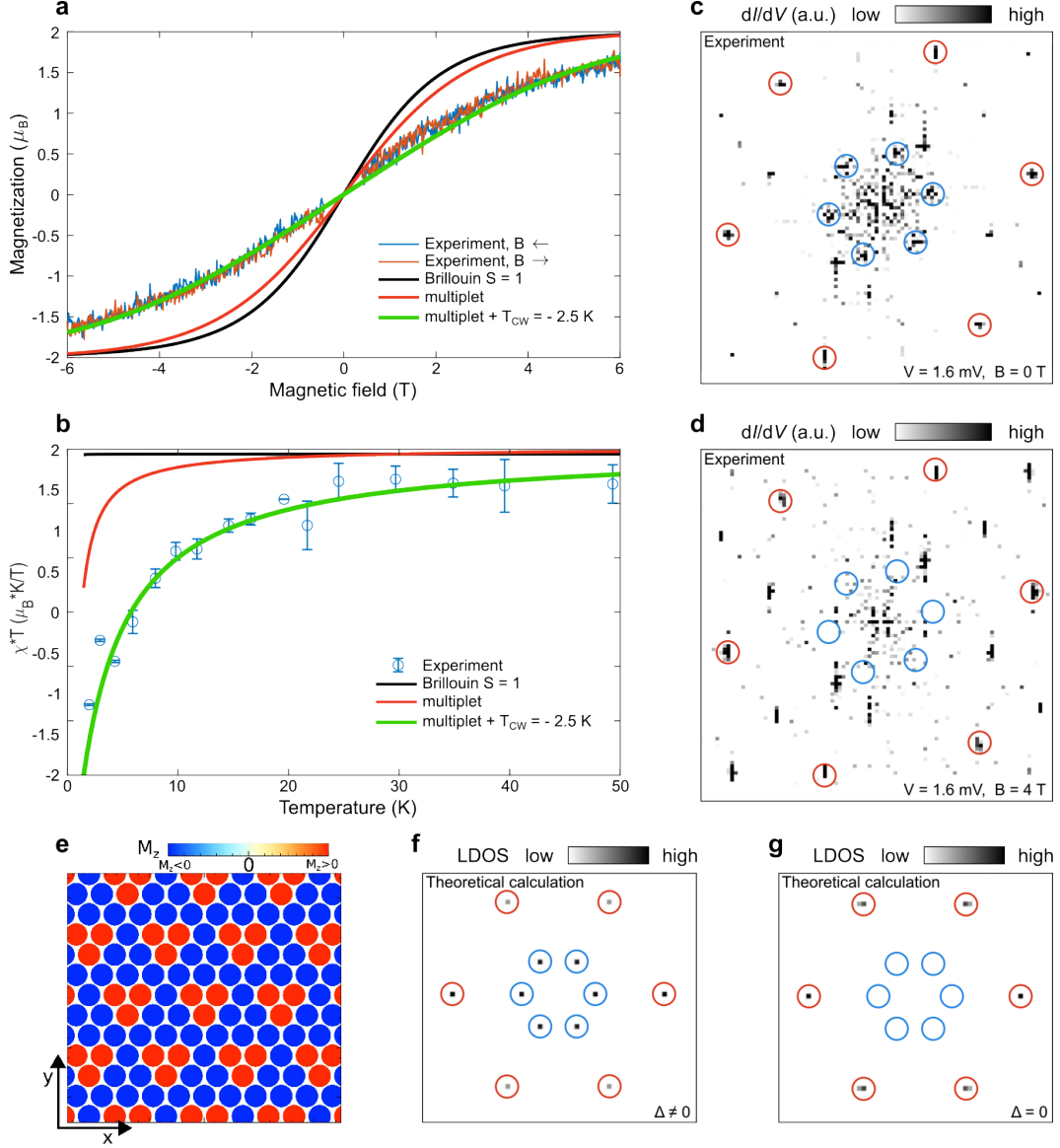


FIG. 4. **Magnetic order of the NiDCA₃ SMC.** **a**, Hysteresis curve at $T = 2.0$ K obtained by measuring the XMCD signal while sweeping the magnetic field. Brillouin curve for $S = 1$ (solid black line), magnetization from the multiplet model (red solid line) and including antiferromagnetic interaction with a Curie-Weiss temperature $T_{CW} = -2.5$ K (green solid line) are shown for comparison. **b**, Temperature dependence of the susceptibility obtained from hysteresis curves at various temperatures and comparison with the related models. **c,d**, $dI/dV(\vec{q}, V)$ measured at the energy of the YSR bands ($V = 1.6$ mV) at 0 Tesla (c) and 4 Tesla (d), acquired at $T = 350$ mK. Red circles correspond to the Bragg peaks and blue circles to 3×3 peaks related to the anti-ferromagnetic order. **e**, Illustration of the 3×3 Ising-like magnetic ground state consistent with our observations. **f**, Simulated LDOS(\vec{q}) of the in-gap Yu-Shiba-Rusinov states, allowing the imaging of the magnetic reconstruction in the YSR bandstructure. **g**, In the absence of superconductivity, the additional peaks are not observed in the LDOS(\vec{q}).

3×3 magnetic order from STM measurements

The combination of antiferromagnetic coupling and a frustrated triangular lattice can give rise to exotic magnetic ground states, such as a quantum spin liquid or 120° Néel order. To determine the ground state of the SMC, we map the periodicity of the YSR signal with STM at a temperature of 350 mK, i.e. below the expected ordering temperature of 1.25K. The STM results in Figs. 4c,d show $dI/dV(\vec{q},V)$, an FFT of a LDOS map at the energy of the YSR bands. The main features here are the Bragg peaks (red circles) and 3×3 peaks (blue circles). Upon applying an external magnetic field of $B = 4$ T, that quenches the NbSe₂ superconductivity [39], the Bragg peaks remain while the 3×3 peaks disappear. This suggests that the 3×3 peaks are connected to the YSR bands that rely on superconductivity. The 3×3 supercell of YSR bands could arise due to a moiré pattern, where the registry of Ni atoms with respect to Se atoms of NbSe₂ repeat on a 3×3 supercell. Similarly, the pattern could appear due to a repeating registry between the Ni atoms and 3×3 CDW of NbSe₂. However, our analysis shows that these cases can be ruled out (see SI for details). Therefore, the supercell is likely to arise from a 3×3 magnetic order of the Ni atoms within the SMC.

Theoretical modeling

To explain how the magnetic reconstruction can be observed in the STM signal, we present in Figs. 4e-g model calculations for a system with magnetic reconstruction shown in Fig. 4e. The magnetic ordering induces an exchange coupling in the underlying substrate, leading to a modulated exchange profile (details shown in the SI). This phenomenology is illustrated here with an Ising-like 3×3 magnetic configuration, realizing a minimal ground state with strong out-of-plane anisotropy. In the case of weaker out-of-plane anisotropy, non-collinear configurations featuring 3×3 periodicity would be consistent with our observations as analyzed in the SI. The magnetic modulation translates into the modulation of the energy of YSR states, reflecting the broken translational symmetry of the magnetic structure. The energy modulation of the YSR states can be visualized as a LDOS modulation at an in-gap energy featuring YSR modes (Fig. 4f). In stark contrast, in the absence of superconductivity or a magnetic superstructure, no additional peaks are observed in the FFT of the $dI/dV(\vec{q},V)$ signal (Fig. 4g, see SI for details). While the STM experiments do not directly probe the magnetism of the SMC, the interplay between magnetism and superconductivity translates the magnetic texture into a spatial modulation of the YSR bands

that can be seen in the STM experiments. This allows visualizing frustrated magnetic orders directly in STM and STS experiments.

Discussion

We have successfully synthesized a magnetic SMC on a quasi-2D superconductor NbSe₂, and investigated its electronic and magnetic properties using STM and XMCD. The STM experiments demonstrate that this heterostructure of a magnetic lattice and a superconductor leads to the emergence of YSR bands spanning the entire unit cell of the SMC. Furthermore, combining XMCD and STM results, we discovered an exotic 3×3 antiferromagnetic order of the SMC. We use STM in a novel and unique way to extract information about the spin texture of the system, which is imprinted in the YSR bands. These results open up an extremely tunable path towards realizing novel quantum phases, such as topological superconductivity or quantum spin liquids using SMC/superconductor heterostructures. Here, the tunability stems from the choice of metal atoms, molecules and the substrate, which allows for a combination of different ingredients for designing a wide range of physical systems.

METHODS

Sample preparation. Sample preparation and STM experiments were carried out in ultrahigh vacuum (UHV) systems with a base pressure of $\sim 10^{-10}$ mbar. The 2H-NbSe₂ single crystal (HQ Graphene, the Netherlands) was cleaved *in-situ* in the vacuum. The supramolecular NiDCA₃ complexes were fabricated by the sequential deposition of 9,10-dicyanoanthracene (DCA, Sigma Aldrich) molecules (evaporation temperature 100 °C) and Ni atoms onto the NbSe₂ substrate held at room temperature. Further annealing the sample at 40°C - 70 °C results in larger self-assembled SMC islands.

STM measurements. After preparation the sample was inserted into the low-temperature STM housed in the same UHV system and subsequent experiments were performed at $T = 5$ K (CreaTec LT-STM) and $T = 350$ mK (Unisoku USM-1300). STM images were taken in the constant-current mode. dI/dV spectra were recorded by standard lock-in detection while sweeping the sample bias in an open feedback loop configuration, with a peak-to-peak bias modulation specified for each measurement and at a frequency of 911 Hz. Most of the experiments were carried out with NbSe₂ coated STM tips prepared as described previously [31].

XAS and XMCD measurements. Circular and linear XAS measurements of the SMC on NbSe₂ were performed on the DEIMOS beamline [40, 41] at the SOLEIL synchrotron, France (proposals number 20210238 and 20220372). The sample was prepared *in situ* by following the same procedure described above and characterized prior to the X-ray experiments using an Omicron VT-STM available at the beamline. The sample was transferred in UHV ($< 1 \times 10^{-9}$ mbar) from the preparation chamber to the XAS measurement stage without breaking the vacuum. The measurements were performed from 2 K to 50 K and at magnetic fields of up to 6.0 T. Circularly and linearly polarized light from the synchrotron source was directed on the sample with the photon beam parallel to the magnetic field either at normal or at grazing (60°) incidence. The circular right (CR) and left (CL) photon polarizations are defined with respect to the photon beam direction while the linear horizontal (LH) and vertical (LV) photon polarizations are defined with respect to the sample surface. All signals have been acquired in total electron yield and normalized at the value of a mesh current placed upstream in the beam line to remove time and energy-related variation of the photon intensity. In addition, all spectra have been normalized to the related pre-edge intensity. Background spectra over the energy range of the Ni $L_{2,3}$ edges were acquired on a clean NbSe₂, normalized to the absorption at the related pre-edge energy, and subtracted from the spectra of sample covered with the SMC. To compare with theory, we normalize both experiment and simulated spectra from multiplet calculation to the integral of the corresponding total XAS. Magnetization loops were acquired by measuring the CR and CL signals at the energy corresponding to maximum absolute value of the XMCD as a function of the magnetic field and obtaining the resulting curve by subtracting CR-CL. The amplitude of the curve was normalized such that the value of M at $T = 2$ K and $B = 6$ T reflects the total magnetic moment obtained from sum rules in normal incidence, i.e. $m = m_S + m_L$. For the shown sample and assuming a $3d^8$ configuration, we find a spin magnetic moment $m_S = 1.32\mu_B$, an orbital magnetic moment $m_L = 0.24 \mu_B$, and $m = 1.56 \mu_B$. Curves measured at higher temperature have been rescaled keeping the ratio with the curve measured at $T = 2$ K. The magnetic susceptibility has been estimated by fitting each magnetization loop with a Brillouin function and taking the slope of the fitted curve at $B = 0$ T.

Multiplet calculations. Spectra of Ni $L_{2,3}$ edges were simulated using the Quanta multiplet code [42] including electron-electron interaction, spin-orbit coupling, crystal field splitting of the 3d orbitals, and Zeeman interaction. Values of the Slater integrals and spin-orbit coupling were obtained using atomic calculations with the Cowan code [43]. Rescaling factors for the 3d-3d and 2p-3d Slater integrals, as well as the relative on-site energy of the 3d orbitals were used as free

parameters to fit the experiments. The fit was performed using a Bayesian optimization algorithm minimizing the sum of the individual mean square error over the set of angular dependent circular and linear absorption spectra. In addition, from the quantum states generated by the multiplet we infer anisotropy parameter D and electron spin g -factor that were used as input for a spin Hamiltonian used to fit the magnetization loop at 2 K and magnetic susceptibility data. We used 2 independent parameters for the electron-electron interaction, 3 independent parameters for the onsite orbital energy, plus an additional parameter to account for the magnetic coupling, see SI for more details. The spectra were calculated taking the imaginary part of the Green functions of the electric dipole transition operator applied to the nickel electron wavefunctions with a Lorentzian broadening of 800 meV and a Gaussian broadening of 200 meV. To reproduce the energy dependent life-time of the X-ray absorption excitation [44] we further applied an additional linear photon energy-dependent Lorentzian broadening ranging from 0.1 eV to 1.2 eV over the Ni L_3 and from 0.6 eV to 2.2 eV over the L_2 edge. The best values obtained from the fit are shown in Table S1.

DFT calculations. First principles calculations were performed using the spin-polarized DFT as implemented as in the periodic plane-wave basis code QUANTUM-ESPRESSO [45]. Van der Waals interactions were included by considering the DFT-D3 functional [46] with a kinetic energy cutoff of 60 Ry, and core electrons were represented by ultra-soft pseudopotentials generated with the Rappe–Rabe–Kaxiras–Joannopoulos (RRKJ) recipe [47]. A Hubbard $U = 3$ eV term was introduced to improve the description of the correlation of the 3d electrons in the Ni atom within the simplified version of Cococcioni and de Gironcoli implemented in QUANTUM-ESPRESSO [48].

ACKNOWLEDGEMENTS

This research made use of the Aalto Nanomicroscopy Center (Aalto NMC) facilities and was supported by the European Research Council (ERC-2017-AdG no. 788185 “Artificial Designer Materials”) and Academy of Finland (Academy professor funding nos. 318995 and 320555, Academy research fellow nos. 331342, 336243 and nos. 338478 and 346654). L.Y. acknowledges support from the Jiangsu Specially-Appointed Professors Program, Suzhou Key Laboratory of Surface and Interface Intelligent Matter (Grant SZS2022011), Suzhou Key Laboratory of Functional Nano & Soft Materials, Collaborative Innovation Center of Suzhou Nano Science & Technology, and the 111 Project. Computing resources from the Aalto Science-IT project and CSC, Helsinki are gratefully acknowledged. A.S.F has been supported by the World Premier International Research Center

Initiative (WPI), MEXT, Japan. S.R, M.K, J.L, and F.D. acknowledge support from the Institute for Basic Science under Grant IBS-R027-D1. We are grateful to Fadi Choueikani for assistance with XAS and XMCD experiments and to the SOLEIL staff for smoothly running the facility. The authors would like to thank Bernard Muller for his significant contribution to the construction of DEIMOS beamline (design and engineering) and Florian Leduc for his support. The MBE chamber used during the XAS/XCMD experiment on DEIMOS has been funded by the Agence National de la Recherche; grant ANR-05-NANO-073.

* Corresponding authors. Email: donati.fabio@qns.science, peter.liljeroth@aalto.fi, lhyang@suda.edu.cn

- [1] Elsa Prada, Pablo San-Jose, Michiel W. A. de Moor, Attila Geresdi, Eduardo J. H. Lee, Jelena Klinovaja, Daniel Loss, Jesper Nygård, Ramón Aguado, and Leo P. Kouwenhoven, “From Andreev to Majorana bound states in hybrid superconductor–semiconductor nanowires,” *Nat. Rev. Phys.* **2**, 575–594 (2020).
- [2] Andres Castellanos-Gomez, Xiangfeng Duan, Zhe Fei, Humberto Rodriguez Gutierrez, Yuan Huang, Xinyu Huang, Jorge Quereda, Qi Qian, Eli Sutter, and Peter Sutter, “Van der Waals heterostructures,” *Nat. Rev. Methods Primers* **2**, 58 (2022).
- [3] Joel Röntynen and Teemu Ojanen, “Topological superconductivity and high Chern numbers in 2D ferromagnetic Shiba lattices,” *Phys. Rev. Lett.* **114**, 236803 (2015).
- [4] Jian Li, Titus Neupert, Zhijun Wang, A. H. MacDonald, A. Yazdani, and B. Andrei Bernevig, “Two-dimensional chiral topological superconductivity in Shiba lattices,” *Nat. Commun.* **7**, 12297 (2016).
- [5] Karsten Flensberg, Felix von Oppen, and Ady Stern, “Engineered platforms for topological superconductivity and Majorana zero modes,” *Nat. Rev. Mater.* **6**, 944–958 (2021).
- [6] Ali Yazdani, Felix von Oppen, Bertrand I. Halperin, and Amir Yacoby, “Hunting for Majoranas,” *Science* **380**, eade0850 (2023).
- [7] Lei Dong, Zi’Ang Gao, and Nian Lin, “Self-assembly of metal–organic coordination structures on surfaces,” *Prog. Surf. Sci.* **91**, 101 (2016).
- [8] Maximilian A. Springer, Tsai-Jung Liu, Agnieszka Kuc, and Thomas Heine, “Topological two-dimensional polymers,” *Chem. Soc. Rev.* **49**, 2007–2019 (2020).
- [9] Wei Jiang, Xiaojuan Ni, and Feng Liu, “Exotic topological bands and quantum states in metal–organic and covalent–organic frameworks,” *Acc. Chem. Res.* **54**, 416–426 (2021).
- [10] Pietro Gambardella, Sebastian Stepanow, Alexandre Dmitriev, Jan Honolka, Frank M.F. De Groot, Magalí Lingenfelder, Subhra Sen Gupta, D. D. Sarma, Peter Bencok, Stefan Stanescu, Sylvain Clair, Stéphane Pons, Nian Lin, Ari P. Seitsonen, Harald Brune, Johannes V. Barth, and Klaus Kern, “Supramolecular control of the magnetic anisotropy in two-dimensional high-spin Fe arrays at a metal interface,” *Nat. Mater.* **8**, 189–193 (2009).

- [11] Jan Girovsky, Jan Nowakowski, Md. Ehesan Ali, Milos Baljovic, Harald R. Rossmann, Thomas Nijs, Elise A. Aeby, Sylwia Nowakowska, Dorota Siewert, Gitika Srivastava, Christian Wäckerlin, Jan Dreiser, Silvio Decurtins, Shi-Xia Liu, Peter M. Oppeneer, Thomas A. Jung, and Nirmalya Ballav, “Long-range ferrimagnetic order in a two-dimensional supramolecular Kondo lattice,” *Nat. Commun.* **8**, 15388 (2017).
- [12] Ignacio Piquero-Zulaica, Jorge Lobo-Checa, Zakaria M. Abd El-Fattah, J. Enrique Ortega, Florian Klappenberger, Willi Auwärter, and Johannes V. Barth, “Engineering quantum states and electronic landscapes through surface molecular nanoarchitectures,” *Rev. Mod. Phys.* **94**, 045008 (2022).
- [13] Zi’Ang Gao, Chia Hsiu Hsu, Jing Liu, Feng Chuan Chuang, Ran Zhang, Bowen Xia, Hu Xu, Li Huang, Qiao Jin, Pei Nian Liu, and Nian Lin, “Synthesis and characterization of a single-layer conjugated metal-organic structure featuring a non-trivial topological gap,” *Nanoscale* **11**, 878 (2019).
- [14] Luh Yu, “Bound state in superconductors with paramagnetic impurities,” *Acta Phys. Sin* **21**, 75–91 (1965).
- [15] Hiroyuki Shiba, “Classical spins in superconductors,” *Prog. Theor. Phys.* **40**, 435–451 (1968).
- [16] A. I. Rusinov, “On the theory of gapless superconductivity in alloys containing paramagnetic impurities,” *Sov. Phys. JETP* **29**, 1101–1106 (1969).
- [17] S. Nadj-Perge, I. K. Drozdov, J. Li, H. Chen, S. Jeon, J. Seo, A. H. MacDonald, B. A. Bernevig, and A. Yazdani, “Observation of Majorana fermions in ferromagnetic atomic chains on a superconductor,” *Science* **346**, 602–607 (2014).
- [18] Yao Lu, Wen Yu He, Dong Hui Xu, Nian Lin, and K. T. Law, “Platform for engineering topological superconductors: superlattices on Rashba superconductors,” *Phys. Rev. B* **94**, 024507 (2016).
- [19] Stephan Rachel, Eric Mascot, Sagen Cocklin, Matthias Vojta, and Dirk K. Morr, “Quantized charge transport in chiral Majorana edge modes,” *Phys. Rev. B* **96**, 205131 (2017).
- [20] Kim Pöyhönen, Isac Sahlberg, Alex Westström, and Teemu Ojanen, “Amorphous topological superconductivity in a Shiba glass,” *Nat. Commun.* **9**, 2103 (2018).
- [21] Lucas Schneider, Philip Beck, Jannis Neuhaus-Steinmetz, Levente Rózsa, Thore Posske, Jens Wiebe, and Roland Wiesendanger, “Precursors of Majorana modes and their length-dependent energy oscillations probed at both ends of atomic Shiba chains,” *Nat. Nanotechnol.* **17**, 384–389 (2022).
- [22] Benjamin W. Heinrich, Jose I. Pascual, and Katharina J. Franke, “Single magnetic adsorbates on s-wave superconductors,” *Prog. Surf. Sci.* **93**, 1–19 (2018).
- [23] Lucas Schneider, Philip Beck, Levente Rózsa, Thore Posske, Jens Wiebe, and Roland Wiesendanger, “Probing the topologically trivial nature of end states in antiferromagnetic atomic chains on superconductors,” *Nat. Commun.* **14**, 2742 (2023).
- [24] Maciej Bazarzik, Roberto Lo Conte, Eric Mascot, Kirsten von Bergmann, Dirk K. Morr, and Roland Wiesendanger, “Antiferromagnetism-driven two-dimensional topological nodal-point superconductivity,” *Nat. Commun.* **14**, 614 (2023).

- [25] Martina O. Soldini, Felix Küster, Glenn Wagner, Souvik Das, Amal Aldarawsheh, Ronny Thomale, Samir Lounis, Stuart S. P. Parkin, Paolo Sessi, and Titus Neupert, “Two-dimensional Shiba lattices as a possible platform for crystalline topological superconductivity,” *Nat. Phys.* (2023), [10.1038/s41567-023-02104-5](https://doi.org/10.1038/s41567-023-02104-5).
- [26] K. J. Franke, G. Schulze, and J. I. Pascual, “Competition of superconducting phenomena and Kondo screening at the nanoscale,” *Science* **332**, 940–944 (2011).
- [27] Nino Hatter, Benjamin W. Heinrich, Michael Ruby, Jose I. Pascual, and Katharina J. Franke, “Magnetic anisotropy in Shiba bound states across a quantum phase transition,” *Nat. Commun.* **6**, 8988 (2015).
- [28] Cristina Mier, Benjamin Verlhac, Leó Garnier, Roberto Robles, Laurent Limot, Nicolás Lorente, and Deung Jang Choi, “Superconducting scanning tunneling microscope tip to reveal sub-millielectronvolt magnetic energy variations on surfaces,” *J. Phys. Chem. Lett.* **12**, 2983–2989 (2021).
- [29] Laetitia Farinacci, Gael Reeht, Felix von Oppen, and Katharina J. Franke, “Yu-Shiba-Rusinov bands in a self-assembled kagome lattice of magnetic molecules,” (2023), [arXiv:2307.09993](https://arxiv.org/abs/2307.09993).
- [30] Gerbold C. Ménard, Sébastien Guissart, Christophe Brun, Stéphane Pons, Vasily S. Stolyarov, François Debontridder, Matthieu V. Leclerc, Etienne Janod, Laurent Cario, Dimitri Roditchev, Pascal Simon, and Tristan Cren, “Coherent long-range magnetic bound states in a superconductor,” *Nat. Phys.* **11**, 1013–1016 (2015).
- [31] Shawulienu Kezilebieke, Marc Dvorak, Teemu Ojanen, and Peter Liljeroth, “Coupled Yu–Shiba–Rusinov states in molecular dimers on NbSe₂,” *Nano Lett.* **18**, 2311–2315 (2018).
- [32] Eva Liebhaber, Lisa M. Rütten, Gaël Reeht, Jacob F. Steiner, Sebastian Rohlf, Kai Rosnagel, Felix von Oppen, and Katharina J. Franke, “Quantum spins and hybridization in artificially-constructed chains of magnetic adatoms on a superconductor,” *Nat. Commun.* **13**, 2160 (2022).
- [33] Avijit Kumar, Kaustuv Banerjee, Adam S. Foster, and Peter Liljeroth, “Two-dimensional band structure in honeycomb metal-organic frameworks,” *Nano Lett.* **18**, 5596–5602 (2018).
- [34] Linghao Yan, Orlando J. Silveira, Benjamin Alldritt, Shawulienu Kezilebieke, Adam S. Foster, and Peter Liljeroth, “Two-dimensional metal-organic framework on superconducting NbSe₂,” *ACS Nano* **15**, 17813–17819 (2021).
- [35] Linghao Yan, Orlando J. Silveira, Benjamin Alldritt, Ondřej Krejčí, Adam S. Foster, and Peter Liljeroth, “Synthesis and local probe gating of a monolayer metal-organic framework,” *Adv. Funct. Mater.* **31**, 2100519 (2021).
- [36] Peter Liljeroth, Ingmar Swart, Sami Paavilainen, Jascha Repp, and Gerhard Meyer, “Single-molecule synthesis and characterization of metal-ligand complexes by low-temperature STM,” *Nano Lett.* **10**, 2475–2479 (2010).
- [37] C. Klewe, M. Meinert, A. Boehnke, K. Kuepper, E. Arenholz, A. Gupta, J.-M. Schmalhorst, T. Kuschel, and G. Reiss, “Physical characteristics and cation distribution of NiFe₂O₄ thin films with high resistivity prepared by reactive co-sputtering,” *J. Appl. Phys.* **115**, 123903 (2014).

- [38] D. C. Johnston, “Magnetic susceptibility of collinear and noncollinear Heisenberg antiferromagnets,” *Phys. Rev. Lett.* **109**, 077201 (2012).
- [39] Shawulienu Kezilebieke, Md Nurul Huda, Viliam Vaňo, Markus Aapro, Somesh C. Ganguli, Orlando J. Silveira, Szczepan Głodzik, Adam S. Foster, Teemu Ojanen, and Peter Liljeroth, “Topological superconductivity in a van der Waals heterostructure,” *Nature* **588**, 424–428 (2020).
- [40] P. Ohresser, E. Otero, F. Choueikani, K. Chen, S. Stanescu, F. Deschamps, T. Moreno, F. Polack, B. Lagarde, J.-P. Daguette, F. Marteau, F. Scheurer, L. Joly, J.-P. Kappler, B. Muller, O. Bunau, and Ph. Saintavit, “DEIMOS: A beamline dedicated to dichroism measurements in the 350–2500 eV energy range,” *Rev. Sci. Instrum.* **85**, 013106 (2014).
- [41] L. Joly, E. Otero, F. Choueikani, F. Marteau, L. Chapuis, and P. Ohresser, “Fast continuous energy scan with dynamic coupling of the monochromator and undulator at the DEIMOS beamline,” *J. Synchrotron Rad.* **21**, 502–506 (2014).
- [42] Maurits W. Haverkort, “Quanta for core level spectroscopy - excitons, resonances and band excitations in time and frequency domain,” *J. Phys.: Conf. Ser.* **712**, 012001 (2016).
- [43] Robert D. Cowan, *The Theory of Atomic Structure and Spectra* (University of California Press, Berkeley, 1981).
- [44] Manfred O. Krause and J. H. Oliver, “Natural widths of atomic K and L levels, $K\alpha$ X-ray lines and several KLL Auger lines,” *J. Phys. Chem. Ref. Data* **8**, 329–338 (1979).
- [45] Paolo Giannozzi, Stefano Baroni, Nicola Bonini, Matteo Calandra, Roberto Car, Carlo Cavazzoni, Davide Ceresoli, Guido L. Chiarotti, Matteo Cococcioni, Ismaila Dabo, Andrea Dal Corso, Stefano de Gironcoli, Stefano Fabris, Guido Fratesi, Ralph Gebauer, Uwe Gerstmann, Christos Gougousis, Anton Kokalj, Michele Lazzeri, Layla Martin-Samos, Nicola Marzari, Francesco Mauri, Riccardo Mazzarello, Stefano Paolini, Alfredo Pasquarello, Lorenzo Paulatto, Carlo Sbraccia, Sandro Scandolo, Gabriele Sclauzero, Ari P. Seitsonen, Alexander Smogunov, Paolo Umari, and Renata M Wentzcovitch, “Quantum Espresso: a modular and open-source software project for quantum simulations of materials,” *J. Phys. Condens. Matter* **21**, 395502 (2009).
- [46] Stefan Grimme, Jens Antony, Stephan Ehrlich, and Helge Krieg, “A consistent and accurate ab initio parametrization of density functional dispersion correction (DFT-D) for the 94 elements H-Pu,” *J. Chem. Phys.* **132**, 154104 (2010).
- [47] Andrew M. Rappe, Karin M. Rabe, Efthimios Kaxiras, and J. D. Joannopoulos, “Optimized pseudopotentials,” *Phys. Rev. B* **41**, 1227–1230 (1990).
- [48] Matteo Cococcioni and Stefano de Gironcoli, “Linear response approach to the calculation of the effective interaction parameters in the LDA + U method,” *Phys. Rev. B* **71**, 035105 (2005).